Subaqueous Sediment Characterization near Oyster Colonies by Means of Side-Scan Sonar Imaging and Portable Free-Fall Penetrometer

Samuel Consolvo, S.M.ASCE[1]; Nina Stark, Ph.D., M.ASCE[2]; Celso Castro-Bolinaga, Ph.D.[3]; Grace Massey, Ph.D.[4]; Steven Hall, P.E., Ph.D.[5]; Matthew Campbell[6]; and Melody Thomas[7]

[1]Dept. of Civil and Environmental Engr., Virginia Tech, VA. E-mail: samueltc@vt.edu
[2]Dept. of Civil and Environmental Engr., Virginia Tech, VA. E-mail: ninas@vt.edu
[3]Dept. of Biological and Agriculture Engr., North Carolina State Univ., NC. E-mail: cfcastro@ncsu.edu
[4]Virginia Institute of Marine Science, VA. E-mail: grace.massey@vims.edu
[5]Dept. of Biological and Agriculture Engr., North Carolina State Univ., NC. E-mail: shall5@ncsu.edu
[6]Dept. of Biological and Agriculture Engr., North Carolina State Univ., NC. E-mail: mdcampb2@ncsu.edu
[7]Dept. of Biological and Agriculture Engr., North Carolina State Univ., NC. E-mail: mathoma6@ncsu.edu

Downloaded from ascelibrary.org by VPI & SU on 07/29/20. Copyright ASCE. For personal use only; all rights reserved.

ABSTRACT

Bivalve colonies are being explored regarding their potential contribution to erosion and scour mitigation. As a first step toward this goal, the in situ conditions of a tidal riverbed around an oyster reef in the Piankatank River in Virginia were investigated using a rotary side-scan sonar (SSS) and a portable free-fall penetrometer (PFFP), among other methods. The field survey was performed on October 4 and 5, 2018, in an area with a radius of approximately 300 meters in the direct vicinity of an oyster reef. The SSS results showed a significant increase (>20%) in the standard deviation of the backscatter intensity where the oyster reef was located, indicating an increased surface roughness. The PFFP results suggested somewhat of an increase of in situ peak friction angles with increasing proximity to the oyster reef. This correlation can be explained by an expected increase in sharp oyster shell fragments near the oyster reef. Thus, the SSS offered clear imaging and a measure of increased surface roughness of the oyster reef, while the PFFP provided insights into changes in sediment behavior in the riverbed surrounding the reef.

INTRODUCTION

The impacts of oyster reefs and mussel beds on flow reduction, and thus, possible erosion from waves and currents, has been recognized and further explored over the last decades (van Leeuwen et al. 2010; Campbell and Hall 2018). Furthermore, it can be hypothesized that the presence of bivalves and their attachment to the riverbed affect the surrounding riverbed sediment properties. The overarching motivation of this study is to explore the impacts of bivalves on surrounding riverbed sediment properties, and thus, the impact on the riverbed's erodibility parameters and its susceptibility to scour. Here, we test the use of a rotary side-scan sonar (SSS) system for imaging and remote characterization of an oyster reef, as well as the use of a portable free-fall penetrometer (PFFP) for the geotechnical investigation of surrounding near-surface sediments.

Side-scan sonars, as well as other imaging sonars, have been used to detect, characterize, and classify benthic life to map the seafloor (Roberts et al. 1999; Allen et al. 2005). This instrument

© ASCE

enables rapid quantification and assessment of oyster reefs to better describe growth patterns which can be useful for the fishing industry. In combination with sampling, side-scan sonars have been used to produce high resolution depictions of the seafloor (Lurton et al. 2015).

Different versions of the PFFP device have been used to measure strength properties of the seabed's uppermost sediment layers (Albatal and Stark 2016). However, the number of studies evaluating the effects benthic life has on the PFFP results appear to be limited. Bilici et al. (2018) suggested benthic life contributes to irregularity in the sediment profile in their investigation.

An evaluation of the variability in the backscatter intensity and sediment strength characteristics in close proximity to an oyster reef has not been studied using a combination of the SSS and PFFP instruments. This represents the gap in knowledge this paper attempts to cover.

A field survey was conducted in the Piankatank River in Virginia on October 4 and 5, 2018 at an artificial oyster reef (Fig. 1). In this paper, we will focus on the following two objectives: (1) introduce the remote sensing techniques used to quantify the morphology of a bivalve colony; and, (2) present spatial variation of the sediment strength in terms of the proximity to a bivalve colony from PFFP tests.

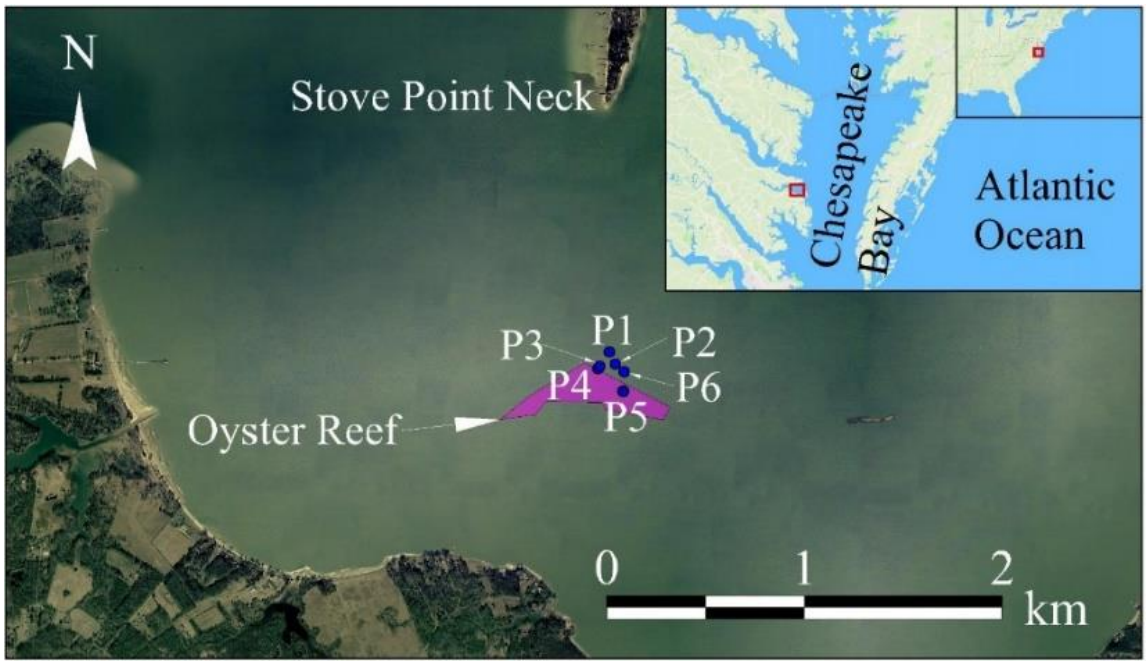

Figure 1. Satellite and map images from Google Earth™ (Data: SIO, NOAA, U.S. Navy, NGA, GEBCO) and Google Maps™ of the Piankatank River field instrument deployments.

REGIONAL CONTEXT

The test site in the Piankatank River is located approximately 95 km east of Richmond, Virginia (Fig. 1). The Piankatank River is an estuarine tributary to the Chesapeake Bay. Natural and artificial oyster reefs are located in the Piankatank, making it a prime location for the tests. The riverbed sediments are highly variable, including combinations of mud, sand, shells, and rock (Lipcius et al. 2010). The riverbed around the artificial oyster reef investigated here was classified primarily as sand or sand/shell, muddy sand/shell, and shell/rock, and the oyster reef is

© ASCE

Downloaded from ascelibrary.org by VPI & SU on 07/29/20. Copyright ASCE. For personal use only; all rights reserved.

located within a zone described as optimal for shell reef restoration (Lipcius et al. 2010). Oyster densities were found to be greater than 100 oysters per square meter in year 2010 (Lipcius et al. 2010). Thereafter, in spring of 2017, granite rock riprap was placed in the Piankatank River to provide new habitat as part of the Chesapeake Bay Oyster Recovery Project (Bloodgood 2017). The oyster reef investigated here (Fig. 1) was created from the aforementioned project.

METHODS

Eleven field instruments were deployed in this study including a *Kongsberg Mesotech Ltd.* 900-1100 kHz SSS (model: 1171 HIRS-HD), a *blueCdesigns blueDrop* PFFP, a *CastAway®* Conductivity, Temperature, and Depth (CTD) probe, two *Nikon CoolPix W300* underwater cameras (C1 and C2), a *GoPro Hero3* underwater camera (C3), a ponar grab sampler, a *RDI 1200 kHz Workhorse* acoustic Doppler current profiler, a *Teledyne RiverPro 1200 kHz* acoustic Doppler current profiler, a *SyQwest Stratabox HD* chirp sub-bottom profiler, and a gravity coring device. Here, results are presented only for the SSS, PFFP, CTD, C3, and the samples collected from the grab sampler. Future work will incorporate the data from the other instruments to better characterize the bivalve colony morphology. Gravity core sampling was attempted, but there was no riverbed sediment successfully retrieved either due to combined effects of early refusal and loss of non-cohesive sediments (a standard orange peel core catcher was used). Table 1 summarizes the field instruments whose data were used in this paper.

Table 1: Summary of field instruments used at each deployment location and relevant data.

Location	P1	P2	P3	P4	P5	P6
Latitude	37.51352	37.51298	37.51283	37.51274	37.51174	37.51262
Longitude	-76.33156	-76.33120	-76.33213	-76.33219	-76.33074	-76.33068
SSS	deployed	deployed	--	--	deployed	--
PFFP: $\overline{qsbc}$ (1) [kPa]	72.3	86.8	93.3	--	hit rock	hit rock
CTD: depth [m]	3.82	3.41	3.39	--	3.24	3.38
Grab Sampler: Classification(2) C_u (3)	SP 1.51	SP 1.46	SP 1.67	--	SP 1.72	SP 1.57

(1) $\overline{qsbc}$ = average of the maximum quasi-static bearing capacities of each deployment per location (see the PFFP section), (2) Sediments were classified using the ASTM Standard D2487-17, and (3) $C_u = D_{60} / D_{10}$, where C_u is the coefficient of uniformity, D_{60} is the grain size at 60% passing, and D_{10} is the grain size at 10% passing

Rotary side-scan sonar (SSS)

The SSS returns an image of the seafloor by emitting pulses of acoustic energy at a selected frequency of 900 kHz over a swath of head angles rotating 360 degrees around a stationary point. Photographs of the instrument setup and a deployment are shown in Figure 2. The reflected sound waves (echoes) are then represented by a backscatter intensity image (Fig. 4) where brighter regions signify areas with high sound reflectivity, and darker regions signify areas with low sound reflectivity. Collier and Brown (2005) and Lurton et al. (2015) both describe brighter regions representative of hard materials and darker regions representative of soft materials.

The backscatter intensity data from the SSS playback were output in 8 bits (2^8) per sample,

© ASCE

Downloaded from ascelibrary.org by VPI & SU on 07/29/20. Copyright ASCE. For personal use only; all rights reserved.

ranging from 0 (0% backscatter—black in color) to 255 (100% backscatter—magenta in color), termed as the Digital Number (DN) by Volgin and Woodside (1996). The DN does not represent an absolute value in units of decibels, but rather, a relative measure of backscattered acoustic energy (Volgin and Woodside 1996). One full rotation (360 degrees) of backscatter intensity data were selected for statistical analysis from test locations P1 and P2 (Fig. 1, Table 1). To determine the distance from the instrument that the DN represents for one head angle, $R = SC \cdot (c_w / SR)$ was used, where R is the radial distance away from the instrument (i.e. range), SC is the sample count, c_w is the speed of sound in water, and SR is the sampling rate. SC and SR are input settings controlled by the user, and c_w was kept to the default value of 1475 m/s. Once R was determined for each DN for each head angle, the inner and outer 20% (i.e., for a 20 m range setting, 0-4 m and 16-20 m) were omitted, leaving the new measurement range at 4 m > R > 16 m. This accounts for the fact that the backscatter intensity data near nadir is artificially higher than the outer range due to the way sound reflects off the seafloor at low incidence angles (Ferrini and Flood 2006). The population standard deviation, σ, of the DN percent values ($\mathrm{DN}_{\%} = 100\% \cdot (\mathrm{DN}/255)$) was then computed for the new ranges and head angles selected and is presented in the results. The DN% values were not normalized against the gain percent value input during the recording of the SSS data. Increasing the gain percent value amplifies the acoustic signal (increasing the acoustic energy), which increases the brightness of the image.

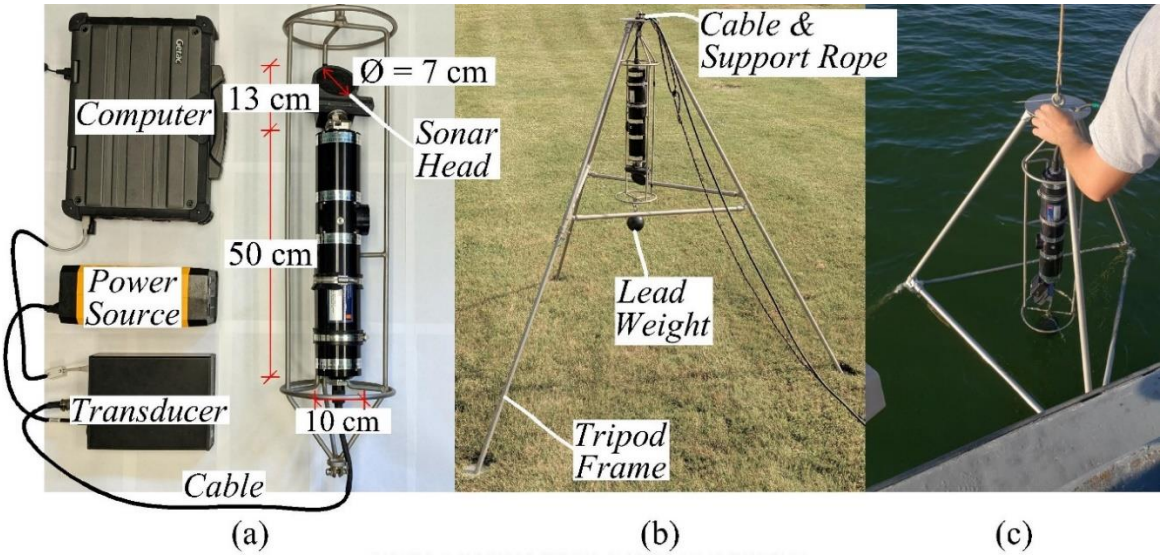

Figure 2. (a) Setup of the SSS instrument. (b) Deployment-ready tripod frame assembly of the SSS. (c) Photograph of the SSS being deployed in the Piankatank River.

Portable free-fall penetrometer (PFFP)

The PFFP was deployed multiple times (4-5) at each of the locations indicated in Table 1. The mass of the PFFP used is approximately 7.4 kg, and the dimensions are shown in Figure 3. The PFFP has five microelectromechanical systems vertical accelerometers that range from ±2 g up to ±250 g and has a dual axis (horizontal) accelerometer limited to ±55 g (where g is the gravitational acceleration) (blueCdesigns ltd. 2015). Deployments where significant horizontal acceleration—where the PFFP did not maintain approximate verticality—was observed were excluded as part of the analyses. The acceleration data is logged at 2 kHz which

© ASCE

Downloaded from ascelibrary.org by VPI & SU on 07/29/20. Copyright ASCE. For personal use only; all rights reserved.

Downloaded from ascelibrary.org by VPI & SU on 07/29/20. Copyright ASCE. For personal use only; all rights reserved.

produces a vertical displacement resolution better than 1 cm (Kiptoo et al. 2019).

The device is released from a vertical position, then free falls under its own weight through the water column until it impacts the riverbed. Penetration depths are typically on the order of 5 cm to greater than 70 cm, where deeper penetrations often correspond to soft mud (Kiptoo et al. 2019) and shallow penetrations often represent dense sandy seabed conditions (Albatal et al. 2019). Upon impact, the sediment resistance force decelerates the PFFP until the velocity is zero. Based on Newton's second law, sediment resistance force, F_{SR}, can be determined by knowing the buoyant unit weight of the penetrometer, W', and the deceleration and mass of the penetrometer, a and m, respectively, given by $F_{SR} = W' - m \cdot a$. This neglects soil buoyancy, side adhesion of the cone, and drag (Stark et al. 2012). The equivalent static cone resistance, $q_{c,eq}$, (also known as the quasi-static bearing capacity, $qsbc$) can then be determined by dividing F_{SR} by the area subjected to load, A, and a strain rate correction, f_{sr}, given by $qsbc = F_{SR} / \left(A \cdot f_{sr} \right)$ (Dayal and Allen 1973; Stark et al. 2011, 2012; Steiner et al. 2014). The logarithmic strain rate correction equation was used, given by $f_{sr} = 1 + K \log_{10} \left(v_{dyn} / v_{ref} \right)$ (Stark et al. 2009), where K is a dimensionless empirical coefficient, v_{dyn} is the dynamic penetration velocity determined from integration of the deceleration profile, and v_{ref} is a reference penetration velocity (0.02 m/s used in this paper which usually corresponds with a Cone Penetration Test (CPT), Albatal et al. 2019). An average was taken of the maximum $qsbc$ values calculated for each deployment using K values of 1.0 and 1.5 based on the similarities in the particle size distribution with Albatal and Stark (2016).

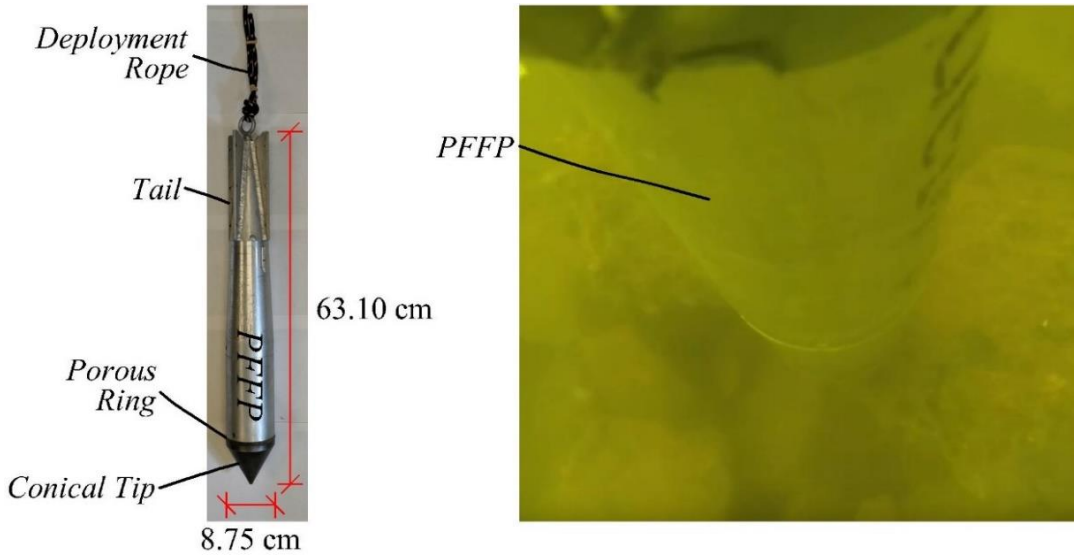

Figure 3. (a) PFFP deployment-ready instrument setup. (b) Still image from a video (C3) taken during one of the deployments at P5 during impact with reef rocks.

To estimate the effective stress angle of internal friction (friction angle), ϕ', based on the PFFP tests, two methods were proposed (Albatal et al. 2019). The first method uses the Durgunoglu and Mitchell (1973) bearing capacity theory where the cone resistance, q_c, is

© ASCE

represented by $q_c = \gamma_s \cdot B \cdot N_{\gamma q} \cdot \zeta_{\gamma q}$ for cohesionless soils, where γ_s is the submerged unit weight of soil (or sediment), B is the cone (or PFFP) diameter, $N_{\gamma q}$ is a bearing capacity factor, and $\zeta_{\gamma q}$ is a shape factor. $N_{\gamma q}$ and $\zeta_{\gamma q}$ are dependent on the friction angle; therefore, iteration is required to determine ϕ' based on a range of reasonably assumed values. The cone resistance is assumed to be $q_c = q_{c,eq} = qsbc$. The steps are outlined in detail in Albatal et al. (2019).

The second method used to determine the friction angle was a correlation developed by Duncan et al. (2014) and given by $\phi' = A + B \cdot D_r - (C + D \cdot D_r)\log_{10}(\sigma'_N / P_a)$, where A, B, C, and D are correlation parameters in degrees that depend on the coefficient of uniformity, D_r is the relative density, σ'_N is the normal stress, and P_a is the atmospheric pressure. The correlation presented in Albatal et al. (2019) was used to determine D_r from the deceleration profile and σ'_N is based on the penetration depth achieved at the maximum $qsbc$. The justifications for using the D_r correlation were based on grain size distribution similarities with the materials analyzed in Albatal et al. (2019) and the low percentage by weight of shell fragments present (average of 3.6%).

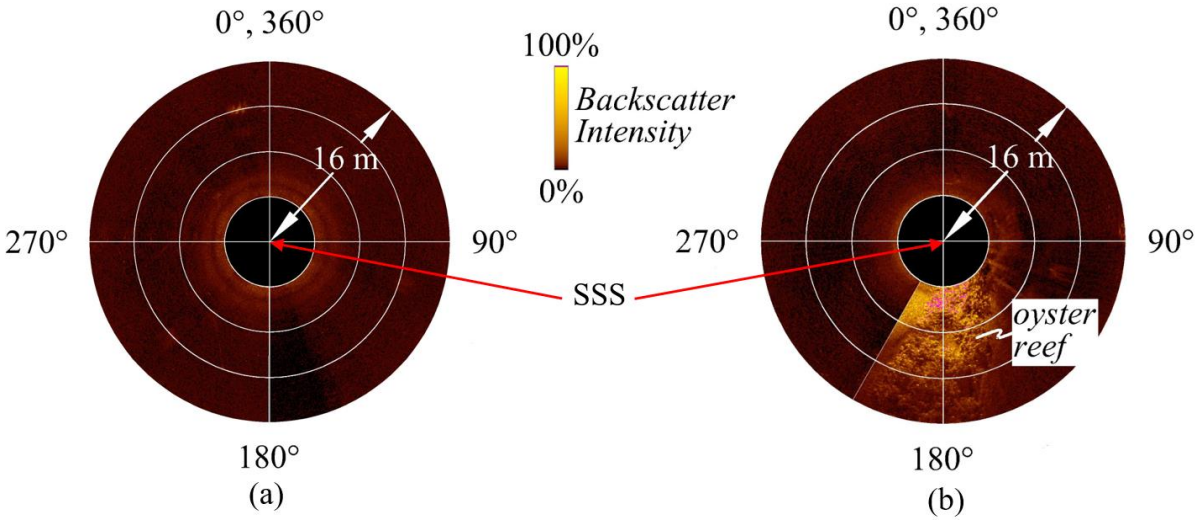

Figure 4: SSS data from location P1 (a) and P2 (b) using the MS1000 Standard PC-based sonar processor (version: 0536 - r6639).

RESULTS

Two of the SSS deployment locations (P1 and P2) were selected for analysis (Fig. 4). The DN% values ranged approximately from 0-34.1% for P1 and 0-100% for P2. The overall average DN% value, μ, was approximately 1.5% for P1 and 2.7% for P2. The standard deviation and coefficient of variation $(c_v = \sigma / \mu)$ of the DN% values were approximately 1.3% and 0.84 for P1, and 7.6% and 2.77 for P2, respectively. The range of gain percent values input during SSS data acquisition was 10-23% for P1 and 12-14% for P2. The head angle with the greatest average DN% value and greatest standard deviation was approximately 54.5° (northeast quadrant) and 346.3° (northwest quadrant) for P1, and both were 183.6° (southeast quadrant) for P2, respectively. Figure 4 is a compass rose color representation of the DN% values for locations P1

© ASCE

Downloaded from ascelibrary.org by VPI & SU on 07/29/20. Copyright ASCE. For personal use only; all rights reserved.

and P2. P1 serves as a control for P2 with little variation in the backscatter intensity as shown in Figure 5. There appears to be an object in the northwest quadrant of the P1 which also corresponds to the greatest standard deviation for the rotation. At P2, there is a clear spike in the standard deviation values between approximately 140° and 207° (Fig. 5) where the subject oyster reef was located. In Figure 4, the azimuth degree value of 0° represents true north as the instrument is equipped with a calibrated compass. The interior black regions represent areas that were omitted from the analysis.

In total, 24 PFFP deployments were carried out, but only 15 were selected for analysis. The deceleration profiles of the remaining 9 deployments indicated the PFFP encountered rock. This occurred exclusively at locations P5 and P6. Figure 6 shows the 15 deployments in terms of relative density versus friction angle and *qsbc* versus friction angle. The computed *qsbc* values and corresponding friction angle values ranged from approximately 43.5-123.8 kPa and 38.0-47.1°, respectively. The range of computed relative density percent values and corresponding friction angle values were approximately 48.4-77.5% and 48.5-54.1°, respectively. The relative density method consistently yielded greater friction angle results than the *qsbc* method. Furthermore, the friction angles for both data sets appeared to increase when approaching the oyster reef (i.e. P3 is closer to the reef than P1 per Figure 1).

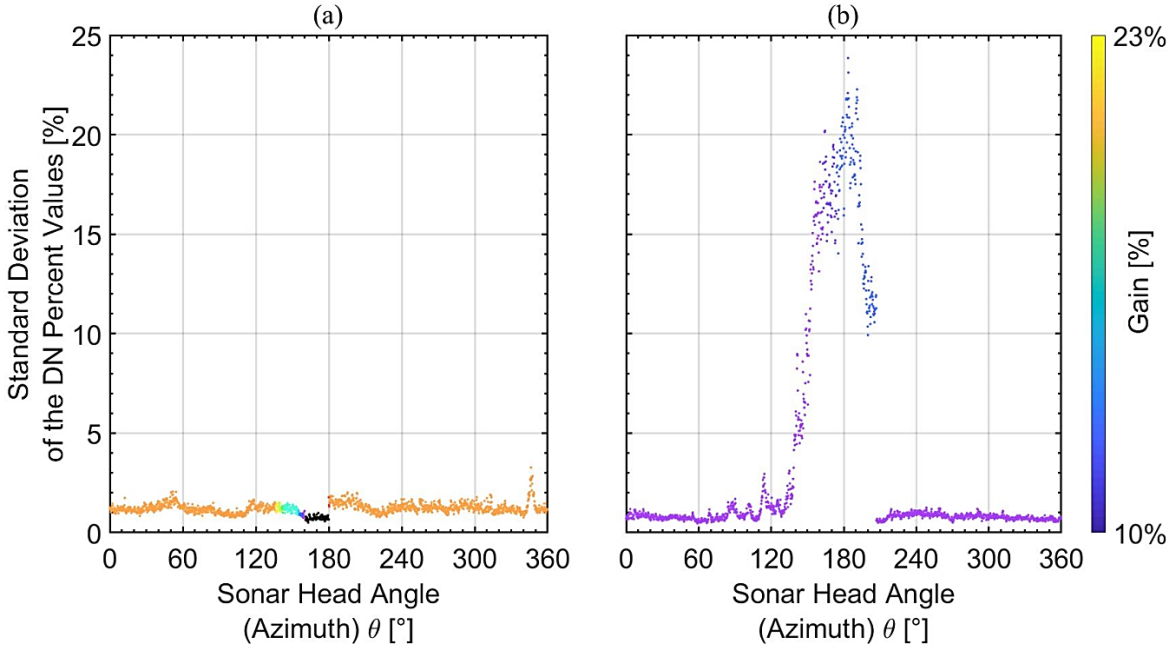

Figure 5. Standard deviation of the DN% values for one rotation (360°) at P1 (a) and P2 (b) of the SSS corresponding to the backscatter intensity images in Figure 4.

DISCUSSION

The SSS image suggests that a high standard deviation of backscatter intensity was indicative of a high surface roughness in terms of particle sizes (Fig. 5b) in line with the study conducted by Collier and Brown (2005). To determine if variable gain settings influenced the σ values, the DN% values were not normalized to any particular gain value. Based on Figure 5, the gain settings did not appear to influence the σ values in any significant way for the range of gain settings applied here.

© ASCE

Downloaded from ascelibrary.org by VPI & SU on 07/29/20. Copyright ASCE. For personal use only; all rights reserved.

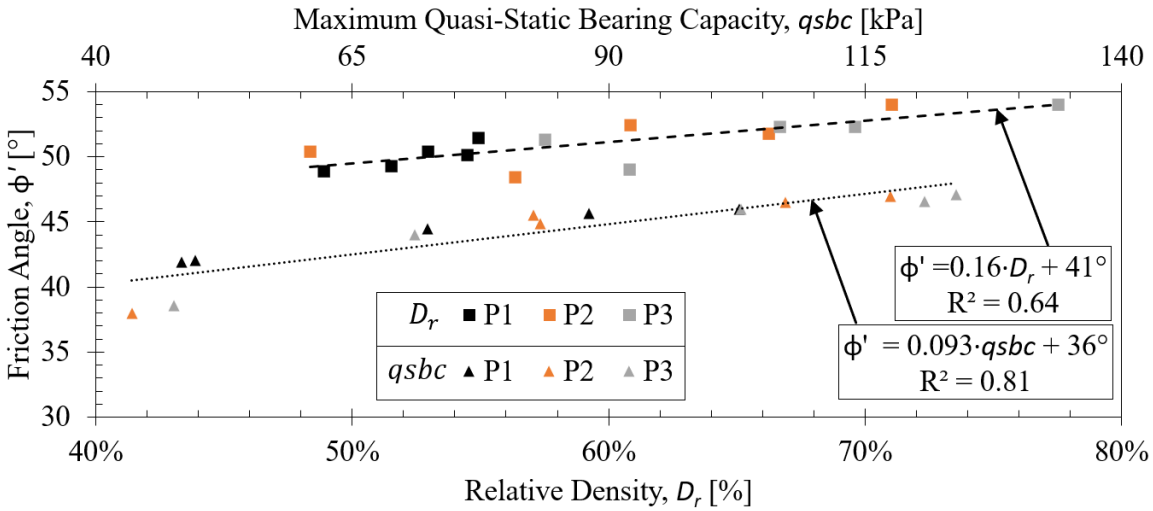

Figure 6. Plot of the maximum *qsbc* and D_r values determined from deceleration profiles of 15 PFFP deployments in the Piankatank River versus the calculated friction angles.

The areas outside of the oyster reef within the range (radius <15 m) of the SSS sites all classified as poorly graded sand. Collier and Brown (2005) suggested a positive correlation between mean particle size and mean backscatter. Considering the standard deviation of C_u was approximately 0.10, sediment samples collected in this field survey can be considered homogeneous. Yet, the values of C_u were higher closer to the oyster reef indicating a greater range of particle sizes, albeit higher on average by only 0.17 relative to P5. The shell fragments (angular and sharp) observed in the samples that were kept in for the sieving analysis potentially explain the increase in C_u closer to the subject oyster reef. In addition to the higher σ values where the oyster reef was located, the grain size distribution from the samples indicated that the material was slightly more coarse. North of the reef, the backscatter intensity and the values of C_u varied little. This suggests that with higher variation in the DN% values, the greater the likelihood that the sediment grain size distribution is well-graded (poorly sorted) relative to the figures presented in this study.

The SSS results may be affected by the chosen default speed of sound (1475 m/s) used during the survey. Based on the salinity levels indirectly measured by the CTD, c_w should have been increased to approximately 1510 m/s (which is approximately 2.3% greater than 1475 m/s). A higher c_w setting would result in a lower R value. Constrained by the way in which the data was acquired, the effects on the backscatter intensity by varying c_w were not carried out in the field. To improve accuracy of the SSS results, future surveys should, if possible, measure salinity levels before deploying the SSS, then adjust c_w in the settings based on the measured levels. Le Bas and Huvenne (2009) suggest a single value of c_w is acceptable for non-navigational sonar mapping, but this does not necessarily justify using a lower value of c_w.

In terms of the PFFP results, the small positive slopes, 0.162 (decimal) for relative density and 0.09 for *qcbc*, can be explained by the SSS results, in that the riverbed sediments appeared to be fairly uniform north of the oyster reef. The closer in proximity the PFFP deployments were to the oyster reef, higher friction angles were observed using both methods (*qsbc* and D_r). The

Downloaded from ascelibrary.org by VPI & SU on 07/29/20. Copyright ASCE. For personal use only; all rights reserved.

© ASCE

range of friction angles appeared to be reasonable, according to Duncan et al. (2014) based on D_{60}, D_{10}, D_r, and the sharpness of shell fragments. The PFFP deployments at P1 through P3 were generally released in the same respective geographic location, but there was some fluctuation as the boat moved around its anchor point. This error could explain the range of D_r and $qsbc$ values at a particular deployment location from natural variation of the riverbed.

Low variability in σ outside the oyster reef from the SSS corresponds to little change in the friction angle (less than 10°) from the PFFP. Therefore, variations in SSS backscatter intensity and variations in PFFP determined that the sediment properties appeared related, and one instrument may be used to predict the uniformity of the results of the other instrument. Investigating a larger spatial grid from an oyster reef could yield further understanding on how the presence of a bivalve colony can affect sediment strength and backscatter intensity variability.

CONCLUSION

A portable free-fall penetrometer (PFFP) and a rotary side-scan sonar (SSS) were among the instruments used to characterize the variability of sediment strength and surface roughness near an artificial oyster reef in the Piankatank River in Virginia. The standard deviation per sonar head angle in the backscatter intensity increased significantly (>20%) where the oyster reef was located, indicating greater surface roughness. The standard deviation values were also used to quantify the variability of surface appearance and roughness on the oyster reef. The PFFP deployments suggested an increase in friction angle from ~45° to ~50° near the oyster reef. This was weakly corroborated by increased particle sizes (mostly shell fragments) in terms of the coefficient of uniformity. Future work should explore both physical changes near natural and artificial reefs and the hydrodynamic and biological implications.

ACKNOWLEDGEMENTS

The authors acknowledge funding from the National Science Foundation through grants CMMI-1820848 and CMMI-1820842. The authors would also like to thank Paul Richardson and Julie Paprocki for fieldwork assistance. For help with extracting the SSS data, the authors would like to thank Ocean Networks Canada, William Lanchantin, and Kongsberg Mesotech Ltd.

REFERENCES

Albatal, A., and Stark, N. (2016). “In-Situ Geotechnical Early Site Assessment of a Proposed Wave Energy Converter Site, Yakutat, Alaska, Using a Portable Free-Fall Penetrometer.” *Geo-Chicago 2016*, ASCE, Chicago, IL, 429-438.

Albatal, A., Stark, N., and Castellanos, B. (2019). “Estimating in-situ relative density and friction angles of nearshore sand from portable free fall penetrometer tests.” *Can. Geotech. J.*, 1-40, doi: https://doi.org/10.1139/cgj-2018-0267.

Allen, Y.C., Wilson, C.A., Roberts, H.H., Supan, J. (2005). “High Resolution Mapping and Classification of Oyster Habitats in Nearshore Louisiana Using Sidescan Sonar.” *Estuar. Coast. Shelf Sci.*, 28(3), 435-446.

ASTM Standard D2487. (2017). *Standard Practice for Classification of Soils for Engineering Purposes (Unified Soil Classification System)*. ASTM International, West Conshohocken, PA, 2017, doi: https://doi.org/10.1520/D2487-17.

Downloaded from ascelibrary.org by VPI & SU on 07/29/20. Copyright ASCE. For personal use only; all rights reserved.

© ASCE

Bilici, C., Stark, N, Hajra, M. G. (2018). "In Situ Geotechnical Characteristics of Surficial Wetland Waterway Sediments." *J. Waterw. Port. Coast.*, ASCE, 144(6), doi: https://doi.org/10.1061/(ASCE)WW.1943-5460.0000462.

Bloodgood, P. (2017). "Reef building to begin on Piankatank River." U.S. Army Corps of Engineers Norfolk District, <https://www.nao.usace.army.mil/Media/News-Stories/Article/1175776/reef-building-to-begin-on-piankatank-river/> (Jun. 1, 2019).

blueCdesigns ltd. (2015). *BlueDrop Operations Manual (v1.100).* Doc. No. 20151119, Halifax, Nova Scotia.

Campbell, M., and Hall, S., (2018). "Hydrodynamic effects on oyster aquaculture systems: A review." *Rev. Aquacult.*, 1-11, doi: https://doi.org/10.1111/raq.12271.

Collier, J., and Brown, C. (2005). "Correlation of sidescan backscatter with grain size distribution of surficial seabed sediments." *J. Mar. Geol.*, 214(4), 431-449.

Dayal, U., and Allen, J. H. (1973). "Instrumented Impact Cone Penetrometer." *Can. Geotech. J.*, 10(3), 397-409.

Duncan, M. J., Wright, S. G., and Brandon, T. L. (2014). *Soil Strength and Slope Stability*. John Wiley & Sons, Inc., Hoboken, NJ.

Durgunoglu, H., and Mitchell, J. K. (1973). *Static Penetration Resistance of Soils*. Research report number NASA-CR-133460, prepared for NASA Headquarters, Washington, D.C.

Ferrini, V. L., and Flood, R. D. (2006). "The effects of fine-scale surface roughness and grain size on 300 kHz multibeam backscatter intensity in sand marine sedimentary environments." *J. Mar. Geol.*, 228(1-4), 153-172.

Kiptoo, D. K., Stark, N., Albatal, A., and Bilici, C. (2019). "Uppermost Subaqueous Soil Variability in Front of the Situk River Inlet, Alaska, from Portable Free Fall Penetrometer." *Geo-Congress 2019*, ASCE, Philadelphia, PA, 71-80.

Le Bas, T., and Huvenne, V. (2009). "Acquisition and processing of backscatter data for habitat mapping – Comparison of multibeam and sidescan systems." *Appl. Acoust.*, 70(10), 1248-1257.

Lipcius, R. N., Shen, J., Schulte, D. M., Hoenig, J. M., and Colden, A. M. (2010). *Ecosystem-Based Planning of Native Oyster Restoration*. Virginia Institute of Marine Science, College of William and Mary, Final Report to U.S. Army Corps of Engineers Norfolk District.

Lurton, X., Lamarche, G., Brown, C., Lucieer, V., Rice, G., Schimel, A., and Weber, T. (2015). *Backscatter measurements by seafloor-mapping sonars. Guidelines and Recommendations*. A collective report by members of the GeoHab Backscatter Working Group.

Roberts, H. H., Wilson, C. A., Supan, J., Winans, W. (1999). "New Technology for Characterizing Louisiana's Shallow Coastal Water Bottoms and Predicting Future Changes." *GCAGS*, 49, 452-461.

Stark, N., Kopf, A., Hanff, H., Stegmann, S., and Wilkens, R. (2009). "Geotechnical Investigations of Sandy Seafloors using Dynamic Penetrometers." Oceans 2009. Biloxi, MS, doi: 10.23919/OCEANS.2009.5422460

Stark, N., Hanff, H., Svenson, C., Enstsen, V. B., Lefebvre, A., Winter, C., and Kopf, A. (2011). "Coupled penetrometer, MBES and ADCP assessments of tidal variations in surface sediment layer characteristics along active subaqueous dunes, Danish Wadden Sea." *Geo-Mar. Lett.*, 31(4), 249-258.

Stark, N., Wilkens, R., Ernstsen, V. B., Lambers-Huesmann, M., Stegmann, S., and Kopf, A. (2012). "Geotechnical Properties of Sandy Seafloors and the Consequences for Dynamic Penetrometer Interpretations: Quartz Sand Versus Carbonate Sand." *Geotech. Geol. Eng.*,

Downloaded from ascelibrary.org by VPI & SU on 07/29/20. Copyright ASCE. For personal use only; all rights reserved.

© ASCE

30(1), 1-14.
Stark, N., Radosavljević, B., Quinn, B., and Hugues, L. (2017). "Application of a portable free-fall penetrometer for the geotechnical investigation of the Arctic nearshore zone." *Can. Geotech. J.*, 54(1), 31-46.
Steiner, A., Kopf, A. J., L'Heureux, J.-S., Kreiter, S., Stegmann, S., Haflidason, H., and Moerz, T. (2014). "In situ dynamic piezocone penetrometer tests in natural clayey soils—a reappraisal of strain-rate corrections." *Can. Geotech. J.*, 51(3), 272-288.
van Leeuwen, B., Augustijn, D.C.M., van Wesenbeeck, B.K., Hulscher, S.J.M.H., de Vries, M.B. (2010). "Modeling the influence of a young mussel bed on fine sediment dynamics on an intertidal flat in the Wadden Sea." *Ecol. Eng.*, 36(2), 145-153.
Volgin, A. V., and Woodside, J. M. (1996). "Sidescan sonar images of mud volcanoes from the Mediterranean Ridge: possible causes of variation in backscatter intensity." *J. Mar. Geol.*, 132(1-4), 39-53.

Downloaded from ascelibrary.org by VPI & SU on 07/29/20. Copyright ASCE. For personal use only; all rights reserved.

© ASCE